RESEARCH BRIEF

Combined Analysis of Antigen Presentation and T-cell Recognition Reveals Restricted Immune Responses in Melanoma

Shelly Kalaora[1], Yochai Wolf[1], Tali Feferman[2], Eilon Barnea[3], Erez Greenstein[2], Dan Reshef[2], Itay Tirosh[1], Alexandre Reuben[4], Sushant Patkar[5], Ronen Levy[1], Juliane Quinkhardt[6], Tana Omokoko[6], Nouar Qutob[1], Ofra Golani[7], Jianhua Zhang[4], Xizeng Mao[4], Xingzhi Song[4], Chantale Bernatchez[8], Cara Haymaker[8], Marie-Andrée Forget[8], Caitlin Creasy[8], Polina Greenberg[1], Brett W. Carter[9], Zachary A. Cooper[4] Steven A. Rosenberg[10], Michal Lotem[11], Ugur Sahin[12], Guy Shakhar[2], Eytan Ruppin[5], Jennifer A. Wargo[4], Nir Friedman[2], Arie Admon[3], and Yardena Samuels[1]

ABSTRACT

The quest for tumor-associated antigens (TAA) and neoantigens is a major focus of cancer immunotherapy. Here, we combine a neoantigen prediction pipeline and human leukocyte antigen (HLA) peptidomics to identify TAAs and neoantigens in 16 tumors derived from seven patients with melanoma and characterize their interactions with their tumor-infiltrating lymphocytes (TIL). Our investigation of the antigenic and T-cell landscapes encompassing the TAA and neoantigen signatures, their immune reactivity, and their corresponding T-cell identities provides the first comprehensive analysis of cancer cell T-cell cosignatures, allowing us to discover remarkable antigenic and TIL similarities between metastases from the same patient. Furthermore, we reveal that two neoantigen-specific clonotypes killed 90% of autologous melanoma cells, both *in vitro* and *in vivo*, showing that a limited set of neoantigen-specific T cells may play a central role in melanoma tumor rejection. Our findings indicate that combining HLA peptidomics with neoantigen predictions allows robust identification of targetable neoantigens, which could successfully guide personalized cancer immunotherapies.

SIGNIFICANCE: As neoantigen targeting is becoming more established as a powerful therapeutic approach, investigating these molecules has taken center stage. Here, we show that a limited set of neoantigen-specific T cells mediates tumor rejection, suggesting that identifying just a few antigens and their corresponding T-cell clones could guide personalized immunotherapy. *Cancer Discov; 8(11); 1366–75. ©2018 AACR.*

[1]Department of Molecular Cell Biology, Weizmann Institute of Science, Rehovot, Israel. [2]Department of Immunology, Weizmann Institute of Science, Rehovot, Israel. [3]Department of Biology, Technion, Haifa, Israel. [4]Departments of Surgical Oncology and Genomic Medicine, The University of Texas MD Anderson Cancer Center, Houston, Texas. [5]Cancer Data Science Lab, National Cancer Institute, NIH, Rockville, Maryland. [6]BioNTech Cell & Gene Therapies GmbH, Mainz, Germany. [7]Department of Life Sciences Core Facilities, Weizmann Institute of Science, Rehovot, Israel. [8]Department of Melanoma Medical Oncology, The University of Texas MD Anderson Cancer Center, Houston, Texas. [9]Department of Diagnostic Radiology, The University of Texas MD Anderson Cancer Center, Houston, Texas. [10]National Cancer Institute, NIH, Maryland. [11]Sharett Institute of Oncology, Hadassah Medical School, Jerusalem, Israel. [12]TRON—Translational Oncology at the University Medical Center of Johannes Gutenberg University GmbH, Mainz, Germany.

Note: Supplementary data for this article are available at Cancer Discovery Online (http://cancerdiscovery.aacrjournals.org/).

J.A. Wargo, N. Friedman, and A. Admon contributed equally to this article.

Corresponding Author: Yardena Samuels, Weizmann Institute of Science, 234 Herzl Street, Wolfson Building, Room 534, Rehovot 76100, Israel. Phone: 972-8-934-3631; Fax: 972-8-934-4373; E-mail: yardena.samuels@weizmann.ac.il

doi: 10.1158/2159-8290.CD-17-1418

INTRODUCTION

Immunotherapy has become a leading cancer treatment, with therapies such as checkpoint blockade now commonly used against many tumor types, and has proven particularly successful in cutaneous melanoma (1). Melanoma cells present on their human leukocyte antigen class I (HLA-I) complex tumor-associated antigens (TAA), which are tissue-specific antigens that are overexpressed in cancer cells, as well as unique mutated antigens, termed neoantigens. Unlike TAAs, which are only differentially expressed, neoantigens are truly unique to the cancerous tissue, thus increasing the likelihood of their recognition by host immune cells, predominantly tumor-infiltrating $CD8^+$ T lymphocytes (2, 3).

Neoantigens have been identified in various tumors and have been shown to be promising immunotherapy targets (4, 5). Mounting evidence suggests that HLA-restricted recognition of neoantigens by T cells contributes to the efficacy of most cancer immunotherapies and provides clues to the extension of immunotherapy to additional cancer types. Furthermore, efforts are under way to develop personalized cancer vaccines based on neoantigen profiles (6–8). Thus, in-depth characterization of the T-cell antigenic targets is of great importance. To this end, we combine in this study HLA peptidomics and a novel neoantigen prediction pipeline with T-cell receptor (TCR) sequencing to comprehensively analyze cancer cell T-cell cosignatures. Although HLA peptidomics directly analyzes the peptides bound to the cells' HLA by LC/MS-MS (6, 9–13), neoantigen prediction based solely on computational tools and subsequent functional screening may skew toward an antigenic profile no longer presented by the cancer cells.

Our research pipeline (Fig. 1) entailed whole-exome sequencing and RNA sequencing (RNA-seq) of 15 melanoma tumor samples derived from 6 patients and 1 melanoma cell line (Supplementary Table S1) in parallel to HLA-peptidome analysis of the HLA-I and HLA-II repertoires on the same tumor cells. Integrating the two data sets revealed the neoantigens and TAAs present in each patient's tumor cells. We found our neoantigen identification approach to be highly complementary to current neoantigen prediction approaches where peptide–HLA-I binding is derived using artificial neural networks (14, 15). In parallel, we isolated tumor-infiltrating lymphocytes (TIL) from each tumor and characterized the T-cell repertoire by TCR sequencing. Neoantigens and TAAs were then tested for their ability to activate TILs to specifically kill melanoma cells using *in vitro* and *in vivo* imaging. The output was a detailed account of the repertoire of neoantigens and TAAs together with TCRβ sequences of their specific TILs.

RESULTS

Identifying Melanoma Germline and Neoantigenic Peptides

Our HLA peptidomics (9, 11) profiling of the melanoma HLA-I and HLA-II antigens from 16 tumor samples (tumor clinical information is provided in Supplementary Table S2; ref. 16) identified 30,496 and 19,932 unique HLA-I–associated and HLA-II–associated peptides, respectively, which were derived from 10,852 and 4,327 different proteins, respectively (Supplementary Tables S3 and S4). Clustering of 8 to 13 amino acid HLA-I peptides identified from each patient showed, as expected, reduced amino acid complexity at the peptides' second and ninth anchor residues (Supplementary Fig. S1A). The length distribution of the identified peptides was consistent with those expected for class I and II HLA peptides (Supplementary Fig. S1B).

Of all the HLA-bound peptides identified using HLA peptidomics, five were neoantigens and 511 and 641 were unique HLA-I and HLA-II TAAs, respectively. Both HLA-I and HLA-II TAAs were derived from 117 different genes (Supplementary Table S5). Neoantigen identification accuracy was validated by comparing the endogenous peptide spectra with synthetic peptide spectra (Supplementary Figs. S2–S4).

High Similarity between HLA Peptidome and TCR Sequence Data of Melanoma Lesions Derived from the Same Patient

Although it is well established that RNA expression profiles of metastases derived from the same patient are highly comparable (Supplementary Fig. S5), similar studies of the HLA peptide repertoires were not previously conducted. We observed substantial overlap among all peptides presented on the cells of different metastases derived from the same patient, with 25% to 80% of peptides detected in at least two metastases from the same patient (Fig. 2A and B; Supplementary Table S6). When comparing TAAs and the total pool of HLA-I (Fig. 2C) and HLA-II (Fig. 2D) peptides derived from two metastases of patient 92, we discovered not only that the metastases presented many of the same peptides but also that their intensities were comparable (r = 0.738 and 0.751 for HLA-I and HLA-II, respectively). This pattern was maintained in all patients and was more significant in HLA-I compared with HLA-II peptides (Supplementary Fig. S6).

Homology of HLA peptide signatures was reflected at the TIL levels, as gathered from our TCRβ chain sequencing analysis (Supplementary Tables S7 and S8). TCR repertoires of the bulk TILs isolated from two metastases of the same patient were similar in clonotype composition and frequency ($P < 0.0001$), whereas TIL repertoires were largely nonoverlapping between patients ($P < 0.01$; Fig. 2E). Further, the most abundant TCR clonotypes in a given patient were found at comparable frequencies in both metastases (Fig. 2F; Supplementary Fig. S7A). Interestingly, the TIL populations differed greatly in their clonality across metastases. The frequencies of the top 1, 10, 50, and 100 most abundant TCRs are plotted in Supplementary Fig. S7B, and the Gini index for TIL clonality is plotted in Supplementary Fig. S7C.

Some TCRs were found to be identical by amino acid sequence in their complementarity-determining region 3 (CDR3) but divergent at the nucleotide level. The two most convergent TCRs in each metastasis were derived from between 2 and 8 different nucleotide sequences (Fig. 2G–H; Supplementary Fig. S8), and these sequences in many cases were generated by different V chains.

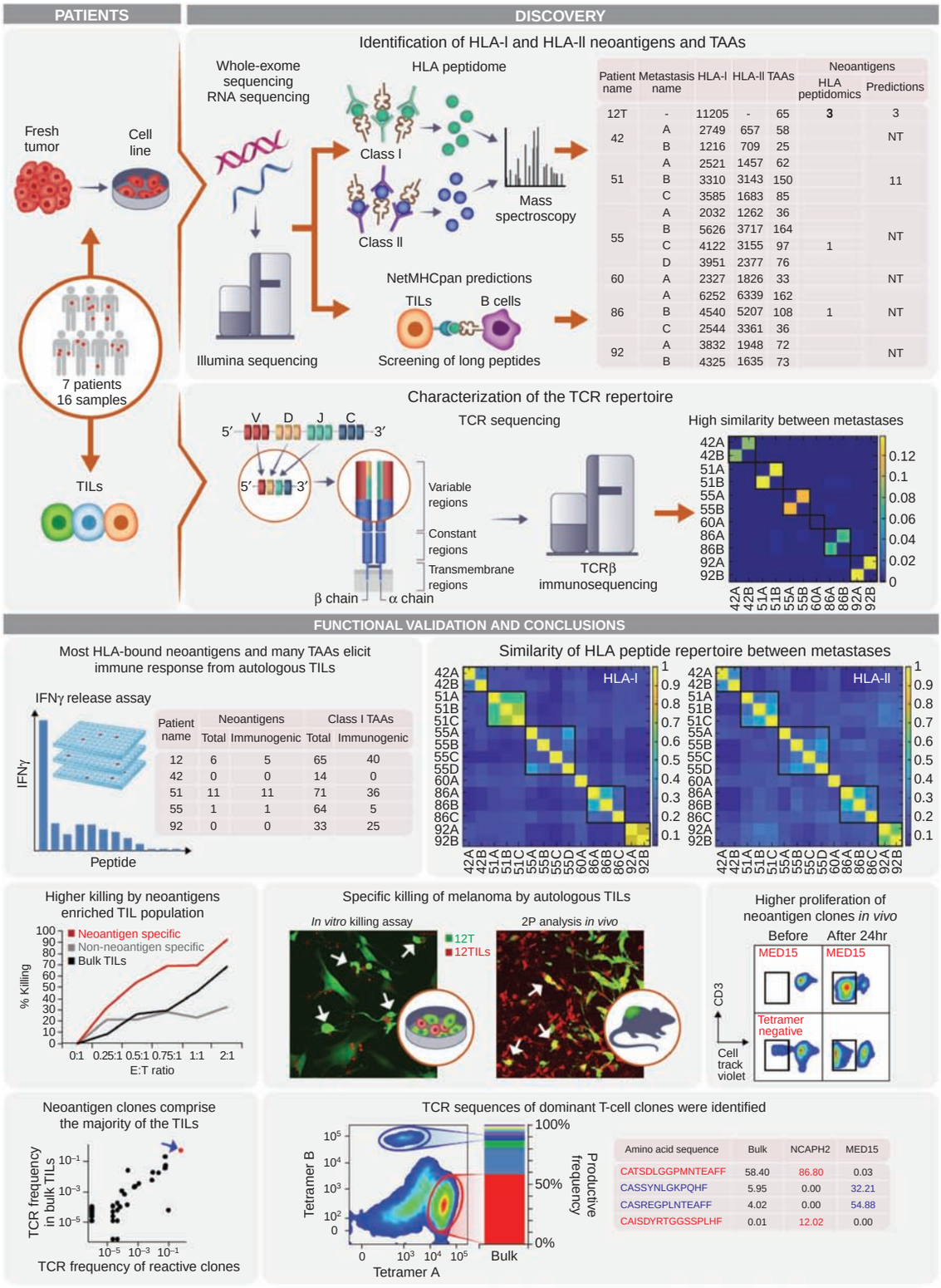

Patient name	Metastasis name	HLA-I	HLA-II	TAAs	Neoantigens: HLA peptidomics	Neoantigens: Predictions
12T	-	11205	-	65	**3**	3
42	A	2749	657	58		NT
	B	1216	709	25		
51	A	2521	1457	62		11
	B	3310	3143	150		
	C	3585	1683	85		
55	A	2032	1262	36		NT
	B	5626	3717	164		
	C	4122	3155	97	1	
	D	3951	2377	76		
60	A	2327	1826	33		NT
86	A	6252	6339	162		
	B	4540	5207	108	1	NT
	C	2544	3361	36		
92	A	3832	1948	72		NT
	B	4325	1635	73		

Patient name	Neoantigens: Total	Neoantigens: Immunogenic	Class I TAAs: Total	Class I TAAs: Immunogenic
12	6	5	65	40
42	0	0	14	0
51	11	11	71	36
55	1	1	64	5
92	0	0	33	25

Amino acid sequence	Bulk	NCAPH2	MED15
CATSDLGGPMNTEAFF	58.40	86.80	0.03
CASSYNLGKPQHF	5.95	0.00	32.21
CASREGPLNTEAFF	4.02	0.00	54.88
CAISDYRTGGSSPLHF	0.01	12.02	0.00

Figure 1. Tumor antigen discovery pipeline. Whole-exome sequencing (WES) of 15 melanoma tumor samples derived from 6 patients and one melanoma cell line was performed in parallel to HLA-peptidome analysis of the cells' HLA-I and HLA-II repertoires. Integrating the WES data with the human proteome database in the mass spectrometry analysis allowed us to reveal the neoantigens and TAAs presented by the patients' tumor cells. In parallel, we applied a neoantigen prediction pipeline followed by a long peptide screen. NT, not tested. TILs isolated from the tumor were sequenced to identify their TCR sequences and reveal any high similarity between the different metastases from the same patient. Neoantigens and TAAs were tested for their reactivity to TILs and the ability of TILs to target the melanoma cells was characterized using *in vitro* and *in vivo* imaging. Neoantigen-specific clones were isolated using tetramers and sequenced to identify their TCR sequence, and TIL reactivity was also derived from their prevalence in the bulk TILs.

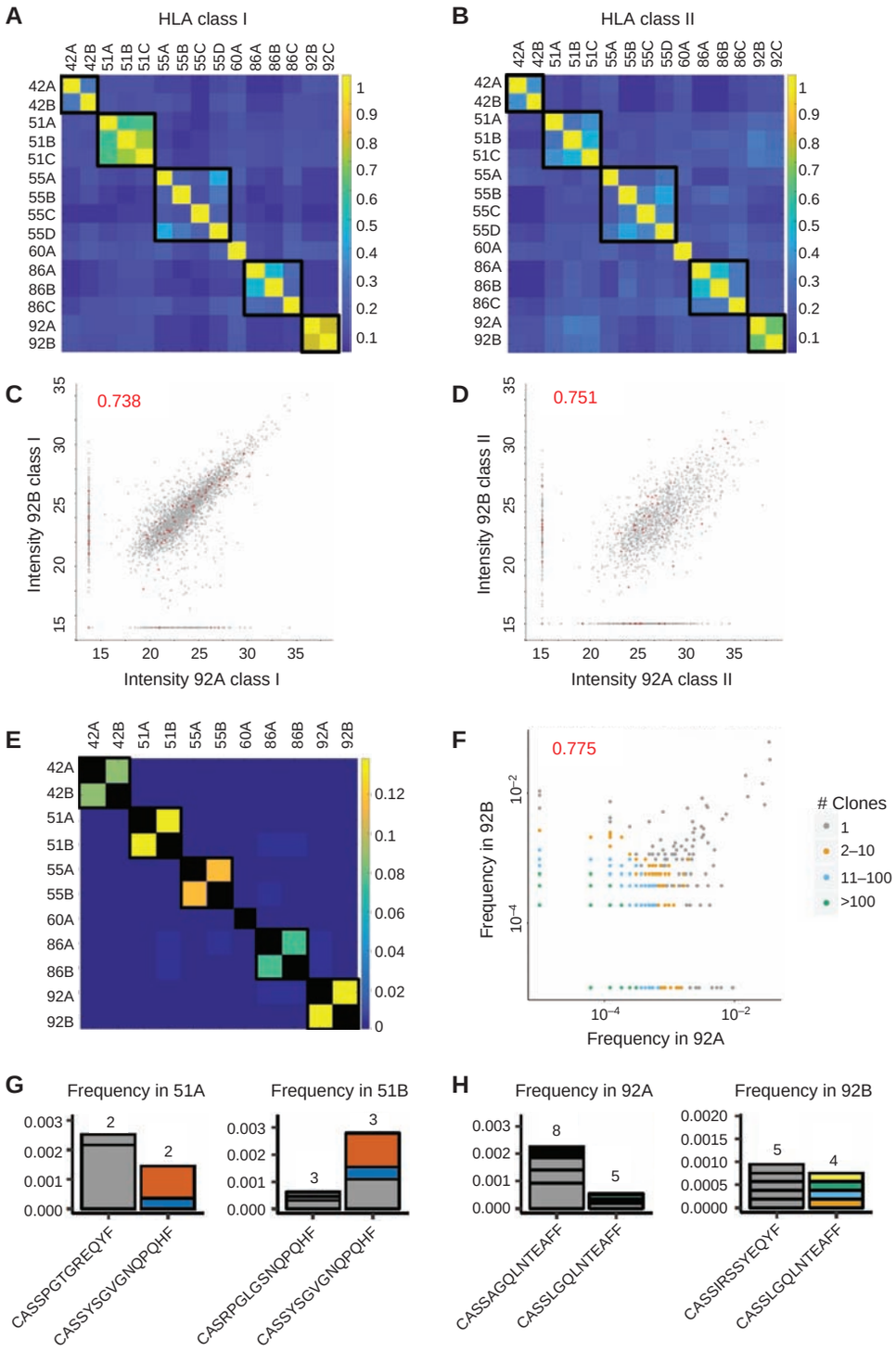

Figure 2. High similarity in the HLA peptides and TCR repertoires of metastases from the same patient. **A** and **B,** Similarity in the heat maps of HLA-I (**A**) and HLA-II (**B**) peptides from the different tumor metastases. Color code indicates the Jaccard index. The highest similarity was observed between metastases from the same patient and between patients with shared HLA alleles. **C** and **D,** The similarity between the presented peptides is observed not only in terms of their identity but also in terms of their intensity. The $\log_2$ of the peptide intensities were plotted for HLA-I (**C**) and HLA-II (**D**) peptides. Unique peptides for each sample were given a constant value of 15. Peptides derived from TAAs are marked in red. Pearson correlations are indicated in red. **E,** Similarity heat maps of the TCR amino acid sequences identified in the various tumor metastases. Color code indicates the Jaccard index. **F,** The frequencies of the various TCRs in the different metastases from the same patient. Because at lower frequencies we found many different TCRs with the same frequency in both metastases, we color-coded the number of TCRs represented by each dot. Pearson correlation is indicated in red. **G–H,** The frequency of the nucleotide sequences of the two most convergent amino acid TCRβ sequences. In patients 51 (**G**) and 92 (**H**), one of the most convergent sequences was detected as most convergent in both metastases. Each nucleotide sequence is represented by layer, with the overlapping sequences presented in the same color in both metastases.

TILs Exhibit High Specificity toward Autologous Melanoma Cells

We chose to focus on the 12T sample as it presented three neoantigens, two of which induced T-cell reactivity. An *in vitro* imaging analysis of CMTMR-labeled 12TIL killing of GFP-tagged 12T melanoma cells revealed that autologous TILs, but not nonautologous counterparts (108TILs), could kill corresponding melanoma cells, with a staggering 50% of all T-cell killing occurring within the first hour of coincubation (Supplementary Fig. S9A–S9B; Supplementary Movies S1–S6).

12TILs induced significant and specific tumor cell death *in vivo*, a finding obtained both with a tumor rejection assay (Supplementary Fig. S10A) and with intravital two-photon microscopy in a mouse model (Supplementary Fig. S10B; Supplementary Movie S7). Interestingly, 12TILs were enriched near the tumor vasculature (Supplementary Fig. S10C; Supplementary Movie S8), had a slower velocity *in vitro* than nonautologous 108TILs (Supplementary Fig. S10D–S10E; Supplementary Movie S9) and exhibited increased clustering relative to 108TILs (Supplementary Fig. S10F), demonstrating their specificity to 12T melanoma cells.

Combining HLA Peptidomic and Antigen Prediction to Identify Immunogenic Neoantigens and TAAs

We further tested the reactivity of TILs to peptides identified by HLA peptidomics by pulsing synthetic peptides onto Epstein–Barr virus (EBV)–transformed B cells expressing matched HLA alleles and coculturing these cells with TILs from the same patient. TIL reactivity was detected for three of the five neoantigens identified by HLA peptidomics: 55DTIL was reactive against a neoantigen derived from oxysterol binding protein-like 8 ($OSBPL8_{D>N}$; Supplementary Fig. S11A). Notably, this neoantigen, which was identified by HLA peptidomics, was predicted to be a weak binder according to NetMHCpan (Supplementary Table S9). 12TIL was reactive against neoantigens derived from mediator complex subunit 15 ($MED15_{P>S}$; ref. 9) and Condensin-2 complex subunit H2 ($NCAPH2_{S>Y}$; Fig. 3A; Supplementary Fig. S11B–S11C). Importantly, only the mutated peptides stimulated TIL release of IFNγ, whereas the wild-type peptides elicited no response. Two neoantigens ($TPD52L2_{S>L}$ from 12T and $TAS2R43_{S>F}$ from 86B) did not induce a detectable IFNγ response in the respective TILs.

To identify neoantigens that may have been missed as they are no longer presented by the tumor or may have been missed by HLA peptidomics, but which had prior immunogenicity by the autologous TILs, we used NetMHCpan to predict the potential binding affinity of all neoantigens to the patient-restricted HLA alleles (14, 15). We then ranked the peptides based on their RNA expression as previously done (8). We then assessed the reactivity of the 50 most highly expressed predicted mutated peptides, using 25-mer synthetic peptides that included the mutation flanked by 12 amino acids on either side to allow for flexibility in the position of the mutated residue within the final processed and presented peptide. We further tested the reactivity of all possible minimal epitopes (derived from the 25-mers) that could be derived from the mutation to identify the exact neoantigen sequence that elicited a TIL response (Fig. 3B; Supplementary Table S10).

Four different 25-mer predicted peptides were reactive for patient 12TILs, and each of these contained one to three different reactive minimal epitopes (Fig. 3B). Minimal epitopes from the same gene that evoked reactivity were found to contain overlapping sequences, suggesting that these may be the core TCR recognition motifs. As seen in Supplementary Fig. S12, all the predicted neoantigen genes were expressed, suggesting that their lack of surface presentation was due to another escape mechanism. Interestingly, minimal epitopes predicted to bind with higher affinity according to NetMHCpan did not elicit T-cell responses (Supplementary Table S11). A similar analysis for patient 51 identified 11 neoantigens: 9 derived from point mutations, 1 from a frame shift mutation (in HLA-DRA), and 1 from a deletion (in MRPL44; Supplementary Fig. S13). As we observed that some predicted 25-mer peptides were processed and bound the HLA allotypes expressed by the 12T and 51A tumors, the prediction algorithms allowed further identification of reactive peptides, emphasizing the complementarity of both systems.

Strikingly, *in vitro* killing assays involving 12T GFP-tagged melanoma cells revealed that the neoantigen-enriched TIL population had an enhanced killing ability of their autologous melanoma cells compared with the bulk TIL population or the neoantigen-negative population (Fig. 3C). TIL reactivity was also observed against many of the TAAs identified by HLA peptidomics (Fig. 3A; Supplementary Fig. S14): 51ATILs, 92BTILs, and 55DTILs demonstrated reactivity against 27 of 73, 24 of 33, and 4 of 64 of the TAAs identified from these patient samples, respectively (Supplementary Fig. S14). Reactive TAAs were found in several metastases of the same patient, though the extent of peptide presentation (seen as intensity) was not an indicator of reactivity

Figure 3. Neoantigen-specific T cells show more reactivity, killing ability, and proliferation *in vitro* and *in vivo*. **A,** IFNγ release measured after overnight coculture of the TILs with EBV-transformed B cells that were pulsed with 10 μM of the peptides that were identified in the HLA peptidomics analysis. **B,** IFNγ release measured after overnight coculture of the TILs with EBV-transformed B cells that were pulsed with 10 μM of the 25-mer peptides. For the reactive 25-mers, we also checked the reactivity of each minimal epitope that was predicted to bind the patients' HLA alleles. **C,** A fluorescence-based *in vitro* assay comparing the killing of 12T melanoma cells by autologous bulk 12TILs, enriched neoantigen TIL population, or the rest of the non-neoantigenic TIL population with an increasing effector:target (E:T) ratio. **D,** Bulk TILs were stained with NCAPH2, MED15, GPNMB, and CDK4 tetramers to evaluate the percentage of the different populations in the bulk TILs. **E,** 12T melanoma cells were cocultured with 12TILs for 24 hours, and later were stained with anti-4-1BB antibody and the two tetramers against the neoantigens. The percentage of reactive and nonreactive T cells for each neoantigen, neoantigen-negative, and bulk TIL are indicated. The mean fluorescence intensity (MFI) of the 4-1BB staining was calculated for the reactive T cells in each population. **F,** Flow cytometry analysis of the different antigen populations in the 12TILs before and after injection to NSG mice with 12T melanoma cells tumor. The first panel shows the percentage of the 12TILs and irrelevant 108TILs in the T-cell mixture. The last three panels are gated only to the violet positive cells (only 12TILs) and show the percentage of T cells in each neoantigen or tetramer-negative population that proliferate. The images are representative for three replicates.

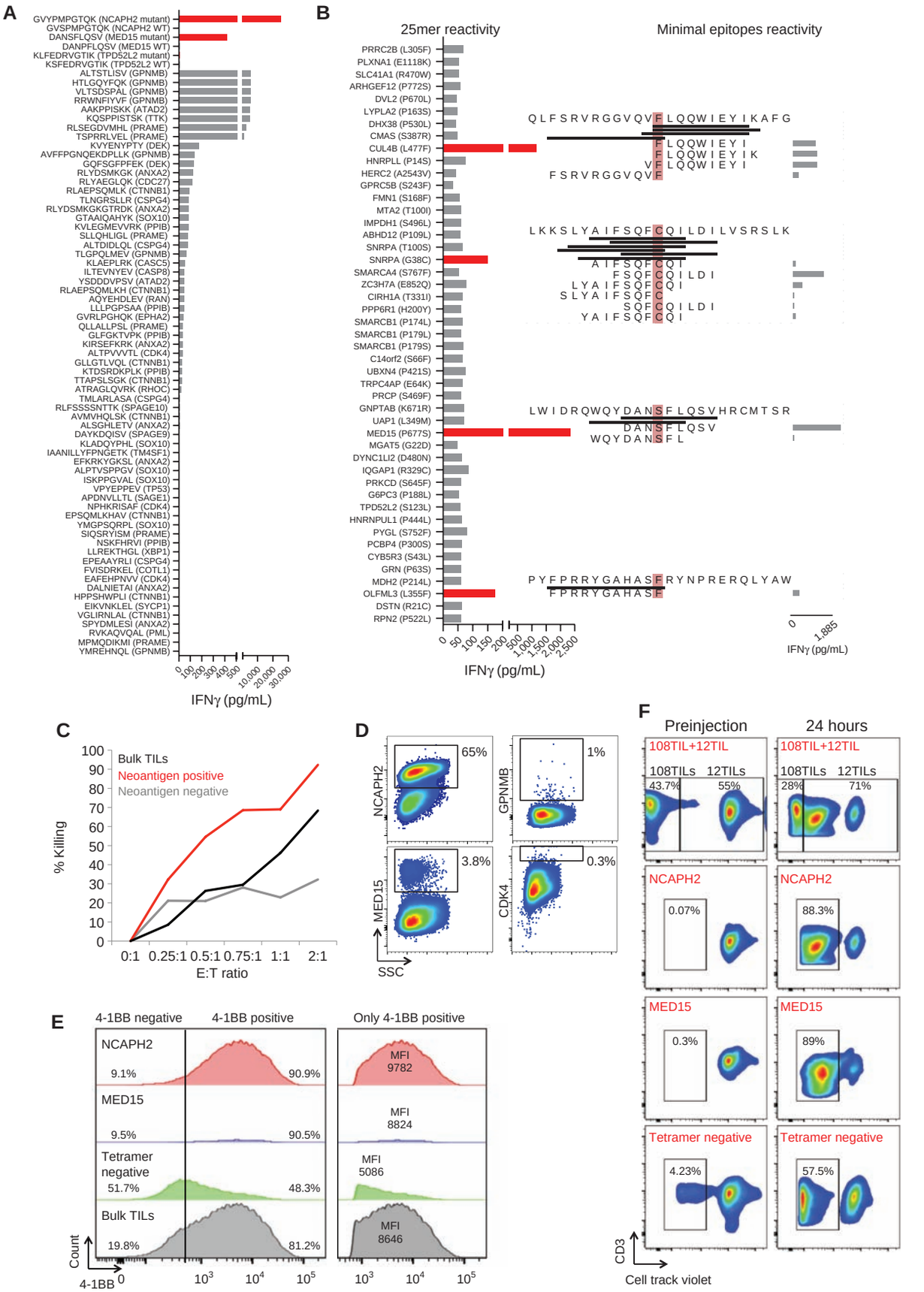

(Supplementary Fig. S14). 42BTILs were not reactive against the identified peptides (tested peptides are listed in Supplementary Table S5).

Neoantigen-Specific T-cell Clone Reactivity and Frequency Affects Neoantigen-Specific TIL Reactivity

Using tetramers specific to the $NCAPH2_{S>Y}$ and $MED15_{P>S}$ neoantigens and two reactive TAAs (ALTSTLISV derived from GPNMB and ALTPVVVTL derived from CDK4), we found that the percentage of tetramer-positive cells in 12TILs was 2.5% for $MED15_{P>S}$, 65.5% for $NCAPH2_{S>Y}$, 1% for GPNMB, and 0.3% for CDK4 (Fig. 3D). To directly estimate the reactivity of neoantigen-specific T cells, we incubated bulk 12TILs with the autologous melanoma cells and stained them with an anti-4-1BB antibody (a marker for T-cell activation) and with the neoantigen tetramers, and analyzed activated T-cell populations by flow cytometry. As seen in Fig. 3E, 4-1BB expression on $NCAPH2_{S>Y}$-reactive T cells [mean fluorescence intensity (MFI) = 9,782, red] and $MED15_{P>S}$-reactive T cells (MFI = 8,824, blue) was higher than the intensity measured for cells reactive to the remainder of antigens presented by the melanoma cells (tetramer-negative, MFI = 5,086, green). Thus, the high TIL response toward the mutant $NCAPH2_{S>Y}$ antigen (Fig. 3A) was due to both a high frequency of $NCAPH2_{S>Y}$-specific T cells and a high level of activation of each neoantigen-specific T cell. The TIL fraction reactive against the melanoma cells was 81% (Fig. 3E).

Our assessment of the abundance of each clone targeting the two identified neoantigens and two TAAs, their IFNγ secretion values, and the finding that neoantigen-reactive clones are more reactive than those targeting TAAs allowed us to roughly estimate that reactive T cells against all neoantigens together accounted for approximately 64.6% of the TILs, those reactive to TAAs accounted for approximately 16.4% of reactive TILs, and the nonreactive T cells accounted for approximately 6.4% of the TILs. Together, our complementary analyses characterized approximately 87.4% of the TIL composition (Supplementary Table S12). The remainder of the TIL population is likely T cells targeting identified nonreactive antigens or other antigens no longer presented by the tumor.

We next evaluated the reactivity of autologous TILs *in vivo*. Mice were inoculated with 12T melanoma cells and an equimolar mixture of 12TILs and 108TILs, where 12TILs were stained with cell track violet to track their proliferation *in vivo*. Twenty-four hours after TIL injection, mouse tumors were processed and analyzed by flow cytometry. TIL proliferation was assessed by cell track violet dilution, and their antigen specificity was assessed using tetramers of the two neoantigens identified in sample 12T. The $NCAPH2_{S>Y}$-specific and $MED15_{P>S}$-specific populations proliferated extensively compared with the tetramer-negative population (Fig. 3F), demonstrating that the neoantigen-specific TILs were the most reactive TIL populations. Our *in vitro* data show a consistent increase in the reactivity of TILs specific to $NCAPH2_{S>Y}$ and $MED15_{P>S}$ compared with TILs reactive to other antigens. Our *in vivo* studies thus demonstrate that neoantigen-specific TILs exhibit a higher level of proliferation compared with both nonautologous and non–neoantigen-specific TILs.

TCR Sequencing Signatures Recapitulate the Neoantigenic Signatures in TILs and Identify Neoantigen-Specific TCR Sequences

To identify the TCR sequences involved in neoantigen-specific TIL reactivity, we used tetramers to isolate $MED15_{P>S}$- and, $NCAPH2_{S>Y}$-binding T cells and T cells unstained by the tetramers. All three populations were sequenced to identify their TCRβ chains. We also sequenced TCRs of reactive and nonreactive TILs by coculturing bulk TILs with autologous melanoma cells and staining for the activation marker 4-1BB. Eleven TCRs (defined by the amino acid sequences of the CDR3 region of TCRβ) dominated across the different samples: 10 were found in the bulk TILs (Supplementary Table S13) and one in sample NCAPH2 (Fig. 4A and B). These 11 TCRs comprised 90.75% to 99.94% of the productive sequences in all sorted samples, and their frequencies ranged from 0.01% to 58.4% in the bulk sample (Fig. 4B). We identified two immunodominant $NCAPH2_{S>Y}$-specific T-cell clonotypes, which accounted for 86.6% (clone 1) and 12% (clone 11) of TILs isolated with the $NCAPH2_{S>Y}$ tetramer. The same TCRβ sequences were enriched in the 4-1BB–positive population compared with the 4-1BB–negative population (Supplementary Fig. S15). We further identified two T-cell clones for the $MED15_{P>S}$ antigen (clones 3 and 4; Fig. 4B). As in the case of $NCAPH2_{S>Y}$, $MED15_{P>S}$ clones were enriched in the 4-1BB–positive population (Supplementary Fig. S15).

Similar to the case of 12T, we identified a reactive TIL clone against the $OSBPL8_{D>N}$ neoantigen identified in tumor 55C, which accounted for 76.11% of 55D TILs, and was the most abundant clone in the 4-1BB positive sample. The TCR sequence of the $OSBPL8_{D>N}$ clone was the third most frequent clone in the 55A tumor (1.48% of TIL population) and the thirty-fourth most frequent in the 55B tumor (0.2% of TIL population), suggesting that this T-cell clone may have played a role in targeting each of the three metastases of this patient to different extents (Supplementary Fig. S16B and Supplementary Table S8).

DISCUSSION

To the best of our knowledge, this is the first report that establishes the antigenic and T-cell landscapes encompassing both the TAAs and neoantigen signatures of metastases derived from the same patient. The significant similarity of the HLA peptidomes between metastases is reflected in the respective TCR signatures. This has strong implications for the process of choosing peptides and TCRs for patient treatment, as it points out that it is clearly essential to identify not only the presented immunogenic peptides, but those of them that are actually common among the patient metastases in order to mediate systemic therapeutic responses in patients with multiple synchronous metastases.

Our study demonstrates that HLA peptidomics, which directly analyzes the peptides bound to the cells' HLA, addresses the need to query neoantigens and TAAs at high levels of accuracy and efficiency. Although neoantigen prediction algorithms could potentially identify all the neoantigens identified by HLA peptidomics, predictions give hundreds, if not thousands, of potential binders without any

A

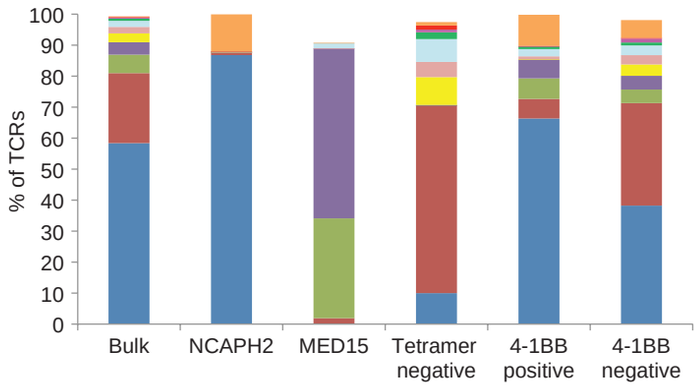

B

Clone	Amino acid sequence	Bulk	NCAPH2	MED15	Tetramer negative	4-1BB positive	4-1BB negative
1	CATSDLGGPMNTEAFF	58.40	**86.80**	0.03	10.00	66.35	38.23
2	CASSLGDPGANVLTF	22.59	0.91	1.88	**60.65**	6.32	33.08
3	CASSYNLGKPQHF	5.95	0.00	**32.21**	0.03	6.63	4.37
4	CASREGPLNTEAFF	4.02	0.00	**54.88**	0.04	6.11	4.43
5	CASSVDPSGANVLTF	2.85	0.06	0.00	8.98	0.02	3.67
6	CASSSFSMGEKLFF	2.10	0.04	0.02	4.90	0.97	3.00
7	CASSLRSSGGFTGELFF	1.95	0.06	1.73	7.37	2.34	3.13
8	CASTSASPKQYF	0.69	0.03	0.00	2.19	0.85	0.95
9	CASNSGDSYGYTF	0.41	0.01	0.00	0.87	0.11	1.23
10	CSARTGTLYEQYF	0.27	0.01	0.00	1.32	0.06	0.28
11	CAISDYRTGGSSPLHF	0.01	**12.02**	0.00	1.11	10.04	5.72

Figure 4. Ten most frequent TCRs in the bulk 12TILs comprise >99% of the TIL population, and the neoantigens are shown to be the most dominant clones. Bulk TILs and five different populations isolated from two different sorting experiments were analyzed using TCR sequencing to identify neoantigen-specific clones and reactive and nonreactive T-cell populations. **A,** Frequency of the top-10 abundant amino acid sequences found in the bulk TILs across the different samples and the second most abundant sequence from NCAPH2. As shown in the bars, these 11 TCRs comprise 90.75%–99.94% of the productive rearrangements in all the samples. **B,** The table indicates the 11 TCR sequences and their frequencies in the different samples. Clones 1 and 11 are against NCAPH2 and clones 3 and 4 are against MED15. Clone 2 is found in the tetramer-negative population and mostly negative to 4-1BB, and therefore probably represents a clone that expended in the tumor but its antigen was downpresented in the tumor cells as part of the immune-editing process.

certainty that any of them are actually presented via the HLA. Researchers must then synthesize and experimentally evaluate potentially thousands of negative peptides to identify tens of positive peptides. Therefore, the advantage of integrating bioinformatic predictions with HLA peptidomics is the elimination of neoantigens that may be false positives identified by bioinformatics. HLA peptidomics, despite its lower sensitivity compared with T cell–based detection assays, further reduces the number of peptides that need to be validated (Supplementary Fig. S17).

The robustness of our neoantigen and corresponding T-cell clone identification strategies is emphasized by the fact that our validated neoantigen-specific T cells kill 90% of their target melanoma cells *in vitro* and *in vivo*. We found that T cells against our identified neoantigens comprise the majority of T cells within the tumor, both in frequency and in reactivity. Most strikingly, our in-depth analysis of the 12T sample detected a mirror image between the magnitude of reactivity of the combined neoantigens and TAAs to the T-cell profile, thus accounting for the majority (~90%) of TIL reactivity. The remaining 10% of TIL reactivity may have been in response to as yet uncharacterized antigens.

Most importantly, the combination of these approaches supports the existence of fewer than expected neoantigens that elicit the response of a restricted set of identifiable neoantigen-specific TILs. Our findings have clear implications for the future development of TIL therapy. Though the low number of identified and validated neoantigens might be unexpected, the responses to these neoantigens were extremely robust, emphasizing that combining strategies for neoantigen identification, such as HLA peptidomics, with approaches that can identify T-cell clones that react to these neoantigens, as we demonstrate here, could significantly increase the efficacy of TIL therapy. Our finding that only a few neoantigen-specific TILs mediate tumor rejection corroborates prior studies that have identified and clinically validated only five or fewer reactive neoantigens per tumor, despite the tumors harboring hundreds or thousands of somatic mutations (5, 17–22). This highlights that although only a few neoantigens and corresponding T-cell clones are present in a tumor, targeting them may be sufficient for patient treatment.

The insight gathered through this analysis strengthens the notion that identification of a few targetable antigens and their corresponding TIL clones could guide personalized cancer immunotherapy. Enriching the infused T cells used for TIL therapy for the combined, yet scant, number of reactive neoantigens and TAAs, using MHC multimer enrichment

(23), RNA vaccines (7, 8, 24), or other expansion protocols to select T-cell populations reactive against patient-specific antigens (5, 25), will greatly personalize this approach and potentially improve the effectiveness of the cancer therapy.

METHODS

Patients and Cells

All patients included in the analysis were diagnosed with metastatic melanoma. Tumor samples were received from 6 different patients treated at The University of Texas MD Anderson Cancer Center who had signed an informed consent for the collection and analysis of their tumor samples. 12T cells and TILs were collected in 2006 and established as described previously (21), with informed patient consent under a protocol approved by the NIH Institutional Review Board (IRB) Ethics Committee. The protocol for 6 tumor samples (from patients 42, 51, 55, 60, 86, and 92) was approved by the MD Anderson IRB (protocol numbers 2012-0846, LAB00-063, and 2004-0069; NCT00338377). Synchronous metastatic tumors were resected via surgery at the same time. The metastases used for the study are described in Supplementary Table S2. Hemotoxylin and eosin staining was generated from OCT-embedded sections, and samples were analyzed for the presence of tumor by a pathologist. Tumor-positive samples were used for subsequent sequencing. The studies were performed after approval by an IRB; the investigators obtained informed written consent from the subjects. All cells have been authenticated by sequencing and were tested routinely for *Mycoplasma* using Mycoplasma EZ-PCR test kit (#20-700-20; Biological Industries, Kibbutz Beit Ha'emek).

Production and Purification of Membrane HLA Molecules

The tumor sample amounts ranged from 0.1 to 0.8 g, and cell-line pellets were collected from 2×10^8 cells. Samples were processed as described previously (9). Full details are provided in the Supplementary Methods.

Prediction of Neoantigens

The NetMHCpan (14, 15) algorithm version 3.0 was used to predict the possible neoantigens from the whole-exome sequencing data (Supplementary Tables S1 and S14). The residues surrounding the amino acids resulting from nonsynonymous mutations were scanned to identify candidate 8–14-mer peptides that were predicted to bind with high affinity (strong binders, %rank ≤ 0.5) or low affinity (weak binders, 0.5 ≤ %rank ≤ 2) to the cells' HLA-I alleles. For samples 12T and 51A, we sorted the peptides according to the RNA expression level of the genes and selected the most highly expressed genes for peptide screens (RNA-seq data are found in Supplementary Table S15 and selected genes are described in Supplementary Table S10). Crude synthetic 25-mer peptides with the mutation in the middle were used to screen point mutations, and overlapping 25-mers (12 amino acids overlap) were used to screen frame shifts. All possible peptides that were predicted to derive from the 25-mer peptides that showed reactivity by the IFNγ release assay were tested to identify the reactive minimal epitopes (Supplementary Table S10).

In Vivo *Mice Assays*

Approval for all the research in mice was granted from the Institutional Animal Care and Use Committee (IACUC) committee at the Weizmann Institute of Science (IACUC #29350816-3).

Additional details regarding patients and cells, production and purification of membrane HLA molecules, identification of eluted HLA peptides, identification of TAAs, analysis of T-cell reactivity by IFNγ release assay, flow cytometry analysis, TCR sequencing, fluorescence-based *in vitro* killing assay, *in vitro* live-cell imaging, *in vivo* rejection assay, live two-photon microscopy of melanoma tumors, calculation of neoantigen and TAA frequencies in TILs, and sequencing of mutations from cDNA are provided in the Supplementary Methods.

Disclosure of Potential Conflicts of Interest

M. Lotem has received honoraria from the speakers bureaus of MSD and BMS and is a consultant/advisory board member for MSD. U. Sahin is CEO at BioNTech, reports receiving a commercial research grant from BioNTech, and has ownership interest (including stock, patents, etc.) in BioNTech. J.A. Wargo has received honoraria from the speakers bureaus of Dava Oncology and Illumina and is a consultant/advisory board member for BMS, Novartis, Genentech, AstraZeneca, Illumina, and Merck. No potential conflicts of interest were disclosed by the other authors.

Authors' Contributions

Conception and design: S. Kalaora, G. Shakhar Y. Samuels
Development of methodology: S. Kalaora, T. Feferman, E. Barnea, U. Sahin, G. Shakhar
Acquisition of data (provided animals, acquired and managed patients, provided facilities, etc.): S. Kalaora, Y. Wolf, T. Feferman, E. Barnea, A. Reuben, J. Quinkhardt, T. Omokoko, C. Haymaker, C. Creasy, B.W. Carter, Z.A. Cooper, M. Lotem, G. Shakhar, J.A. Wargo, A. Admon
Analysis and interpretation of data (e.g., statistical analysis, biostatistics, computational analysis): S. Kalaora, Y. Wolf, T. Feferman, E. Barnea, E. Greenstein, D. Reshef, I. Tirosh, A. Reuben, S. Patkar, R. Levy, J. Quinkhardt, T. Omokoko, N. Qutob, O. Golani, J. Zhang, X. Mao, X. Song, B.W. Carter, G. Shakhar, E. Ruppin, N. Friedman Y. Samuels
Writing, review, and/or revision of the manuscript: S. Kalaora, Y. Wolf, E. Barnea, E. Greenstein, D. Reshef, A. Reuben, C. Haymaker, B.W. Carter, G. Shakhar, J.A. Wargo, N. Friedman, A. Admon, Y. Samuels
Administrative, technical, or material support (i.e., reporting or organizing data, constructing databases): S. Kalaora, J. Quinkhardt, T. Omokoko, C. Bernatchez, M.-A. Forget, P. Greenberg, S.A. Rosenberg, U. Sahin
Study supervision: S. Kalaora, Y. Samuels
Other [developed the imaging strategy (*in vivo* and *in vitro*), performed the *in vivo* imaging, developed the analysis strategy for the imaging, and wrote the relevant details in the manuscript]: T. Feferman

Acknowledgments

We would like to acknowledge the NIH Tetramer Facility for their help in producing the tetramers used in the study, and the Genomics and Bioinformatic units at the Israel National Center for Personalized Medicine (INCPM) for help with sample preparation, sequencing, and analyzing the data. We thank The University of Texas MD Anderson Cancer Center clinical TIL lab for processing of tumor specimens. Also, we thank Tali Wiesel for her help with graphics. This work was supported by the Intramural Research Programs of the National Cancer Institute. Y. Samuels is supported by the Israel Science Foundation grant number 696/17. This project has received funding from the European Research Council (ERC) under the European Union's Horizon 2020 research and innovation program (grant agreement No. 754282), the ERC (StG-335377), the MRA (#402024), the Minerva Foundation Grant, the Knell Family, and the Hamburger Family. Y. Wolf is supported by the Feinberg School Dean's Scholarship. J. Wargo is supported by generous philanthropic contributions to the University of Texas MD Anderson Moon Shots Program for support of tumor line generation.

Received December 18, 2017; revised February 26, 2018; accepted August 16, 2018; published first September 12, 2018.

REFERENCES

1. Topalian SL, Drake CG, Pardoll DM. Immune checkpoint blockade: a common denominator approach to cancer therapy. Cancer Cell 2015; 27:450–61.
2. Tran E, Robbins PF, Rosenberg SA. 'Final common pathway' of human cancer immunotherapy: targeting random somatic mutations. Nat Immunol 2017;18:255–62.
3. Schumacher TN, Schreiber RD. Neoantigens in cancer immunotherapy. Science 2015;348:69–74.
4. Stronen E, Toebes M, Kelderman S, van Buuren MM, Yang W, van Rooij N, et al. Targeting of cancer neoantigens with donor-derived T cell receptor repertoires. Science 2016;352:1337–41.
5. Gros A, Parkhurst MR, Tran E, Pasetto A, Robbins PF, Ilyas S, et al. Prospective identification of neoantigen-specific lymphocytes in the peripheral blood of melanoma patients. Nat Med 2016;22: 433–8.
6. Gubin MM, Artyomov MN, Mardis ER, Schreiber RD. Tumor neoantigens: building a framework for personalized cancer immunotherapy. J Clin Invest 2015;125:3413–21.
7. Ott PA, Hu ZT, Keskin DB, Shukla SA, Sun J, Bozym DJ, et al. An immunogenic personal neoantigen vaccine for patients with melanoma. Nature 2017;547:217–21.
8. Sahin U, Derhovanessian E, Miller M, Kloke BP, Simon P, Lower M, et al. Personalized RNA mutanome vaccines mobilize poly-specific therapeutic immunity against cancer. Nature 2017;547:222–6.
9. Kalaora S, Barnea E, Merhavi-Shoham E, Qutob N, Teer JK, Shimony N, et al. Use of HLA peptidomics and whole exome sequencing to identify human immunogenic neo-antigens. Oncotarget 2016;7: 5110–7.
10. Khodadoust MS, Olsson N, Wagar LE, Haabeth OA, Chen B, Swaminathan K, et al. Antigen presentation profiling reveals recognition of lymphoma immunoglobulin neoantigens. Nature 2017; 543:723–7.
11. Bassani-Sternberg M, Braunlein E, Klar R, Engleitner T, Sinitcyn P, Audehm S, et al. Direct identification of clinically relevant neoepitopes presented on native human melanoma tissue by mass spectrometry. Nat Commun 2016;7:13404.
12. Yadav M, Jhunjhunwala S, Phung QT, Lupardus P, Tanguay J, Bumbaca S, et al. Predicting immunogenic tumour mutations by combining mass spectrometry and exome sequencing. Nature 2014; 515:572–6.
13. Abelin JG, Keskin DB, Sarkizova S, Hartigan CR, Zhang W, Sidney J, et al. Mass spectrometry profiling of HLA-associated peptidomes in mono-allelic cells enables more accurate epitope prediction. Immunity 2017;46:315–26.
14. Hoof I, Peters B, Sidney J, Pedersen LE, Sette A, Lund O, et al. NetMHCpan, a method for MHC class I binding prediction beyond humans. Immunogenetics 2009;61:1–13.
15. Nielsen M, Andreatta M. NetMHCpan-3.0; improved prediction of binding to MHC class I molecules integrating information from multiple receptor and peptide length datasets. Genome Med 2016;8:33.
16. Reuben A, Spencer CN, Prieto PA, Gopalakrishnan V, Reddy SM, Miller JP, et al. Genomic and immune heterogeneity are associated with differential responses to therapy in melanoma. npj Genomic Med 2017;2:10.
17. Robbins PF, Lu YC, El-Gamil M, Li YF, Gross C, Gartner J, et al. Mining exomic sequencing data to identify mutated antigens recognized by adoptively transferred tumor-reactive T cells. Nat Med 2013; 19:747–52.
18. Tran E, Ahmadzadeh M, Lu YC, Gros A, Turcotte S, Robbins PF, et al. Immunogenicity of somatic mutations in human gastrointestinal cancers. Science 2015;350:1387–90.
19. Cohen CJ, Gartner JJ, Horovitz-Fried M, Shamalov K, Trebska-McGowan K, Bliskovsky VV, et al. Isolation of neoantigen-specific T cells from tumor and peripheral lymphocytes. J Clin Invest 2015;125: 3981–91.
20. Pritchard AL, Burel JG, Neller MA, Hayward NK, Lopez JA, Fatho M, et al. Exome sequencing to predict neoantigens in melanoma. Cancer Immunol Res 2015;3:992–8.
21. Lu YC, Yao X, Li YF, El-Gamil M, Dudley ME, Yang JC, et al. Mutated PPP1R3B is recognized by T cells used to treat a melanoma patient who experienced a durable complete tumor regression. J Immunol 2013;190:6034–42.
22. Tran E, Turcotte S, Gros A, Robbins PF, Lu YC, Dudley ME, et al. Cancer immunotherapy based on mutation-specific CD4+ T cells in a patient with epithelial cancer. Science 2014;344:641–5.
23. Schmitt A, Tonn T, Busch DH, Grigoleit GU, Einsele H, Odendahl M, et al. Adoptive transfer and selective reconstitution of streptamer-selected cytomegalovirus-specific CD8+ T cells leads to virus clearance in patients after allogeneic peripheral blood stem cell transplantation. Transfusion 2011;51:591–9.
24. Kranz LM, Diken M, Haas H, Kreiter S, Loquai C, Reuter KC, et al. Systemic RNA delivery to dendritic cells exploits antiviral defence for cancer immunotherapy. Nature 2016;534:396–401.
25. Chen DS, Mellman I. Elements of cancer immunity and the cancer-immune set point. Nature 2017;541:321–30.